Mössbauer, infrared and X-ray Studies of $Ni_{0.5}Zn_{0.5}Cr_xFe_{2-x}O_4$ ferrites

M. A. Amer[1], T. M. Meaz[1*], S. Ata-Allah[2], S. Aboul-Enein[1], and M. O. Abd-El-Hamid[3].

[1-]Physics Department, Faculty of Science, Tanta University, Tanta, Egypt.
[2-]Reactor and Neutron physics Department, Nuclear Research Center, Atomic Energy Authority, Cairo, Egypt.
[3-] Physics Department, Faculty of Science, Minia University, Minia, Egypt.

Spinel ferrites of the system $Ni_{0.5}Zn_{0.5}Cr_xFe_{2-x}O_4$, $0 \le x \le 1$, have been studied using the Mössbauer, IR and X-ray patterns. The Mössbauer spectra showed two broad sextets and a central paramagnetic phase. The spectra have been analyzed to two magnetic sites A and B and two quadrupole doublets C_A and C_B. Both A and C_A are assigned to F^{3+} ions at the tetrahedral A-site, while B and C_B to Fe^{3+} and Fe^{2+} representing the octahedral B-site. The obtained hyperfine interaction parameters: the isomer shifts, quadrupole splittings, outermost line widths, hyperfine magnetic fields and bulk magnetization, are discussed as functions of the Cr^{3+} content (x). The cation distributions of the compounds are estimated using the site preference of the elements and the area ratio of B- to A- sites. Five absorption bands were observed in the infrared spectra in the range between 1100 and 200 cm^{-1}. The refractive index, the IR velocity in the samples and the jump rate of the lattice vacancies have been determined and discussed as functions of molar ratio (x). The Jahn-Teller effect of the Fe^{2+}, Ni^{2+} and/or Cr^{4+} ions has been observed. From X-ray analysis, the true and theoretical lattice parameters, the oxygen parameter and the ionic radii, bonds, edges and hopping lengths of the A- and B-sites have been calculated and discussed depending on the Cr^{3+} ion content (x). The hyperfine fields at the A- and B-sites were found to be dependent on the Cr^{3+} ion content.

**Corresponding author e-mail tmeaz@yahoo.com*

1. Introduction:

Spinel ferrites are still one of the basic materials of modern electronics and computer techniques. Ni-Zn ferrites are attractive for devices of microwave and radio frequency and their applications owing to their high resistivity, mechanical hardness, and high Curie temperature and chemical stability [1-3]. In earlier works some authors, investigated the effect of some additives and substitutions on the physical properties of Ni-Zn ferrites required for high frequency technique [1-3]. It has been found that the main physical properties of spinel ferrites arise from the cationic distribution amongst the tetrahedral A- and octahedral B-sites [4, 5]. The parameters related to the ionic charge and radius, crystal fields play an important role in the site preference of the cations. The effect of Cr^{3+} substitution for Fe^{3+} in spinel ferrites has been studied extensively [6-8]. The results showed that Cr ions are in the charge state Cr^{3+} and intensively occupy the B-sites. When Cr^{3+} is progressively replaced by Fe^{3+} ions, the crystal structure becomes a cubic spinel structure and its Neél temperature increases. The addition of Cr^{3+} ions gives interesting Mössbauer and IR spectra and drastically changes the magnetic hyperfine fields and other Mössbauer, IR and X-ray parameters. Consequently, the aim of the present work is to study the effect of Cr^{3+} substitution for Fe^{3+} on the physical properties of the spinel system $Ni_{0.5}Zn_{0.5}Cr_xFe_{2-x}O_4$, $0 \leq x \leq 1$. The techniques used in this study are the Mössbauer, infrared and X-ray diffraction spectrometers.

2. Experimental:

The spinel samples of the system $Ni_{0.5}Zn_{0.5}Cr_xFe_{2-x}O_4$, with x = 0, 0.2, 0.4, 0.6, 0.8 and 1, were prepared by the usual ceramic technique. High purity oxides of NiO, ZnO, Cr_2O_3 and Fe_2O_3 have been used. The powdered samples were presintered at 1000 ^oC for one day. Finally the powder samples were pressed into pellets and sintered at 1200 ^oC for one day and quenched at room temperature in the normal atmosphere.

The X-ray diffraction patterns were taken using a Shimadzu X-ray diffractometer XD-3, where a copper k_α in the X-ray tube target was used. The recorded reflection planes, as shown in Fig. (1), are (220), (311), (222), (400), (422), (511), (440) and (622). Consequently, the appearance of these reflection planes proved that all the prepared samples have cubic spinel structure. The lattice parameter *a* was determined as indicated previously [9]. The values of the lattice parameter *a* for all samples lie between 8.359 and 8.579 Å, and of the interplanar distance *d* between 1.275 and 3.025 Å, which agree with that obtained previously [6, 9], and ASTM cards.

Figure (2) shows the recorded Mössbauer spectra obtained at room temperature. The Mössbauer spectrometer of the electromechanical type was used in the constant-acceleration mode. The source was ^{57}Co (up to 50 mCi) in Rh matrix at room temperature, where a metallic iron foil was used for calibration. The spectra were analyzed using the least squares fit computer program. However, two magnetic sextet A and B and two quadrupole doublets C_A and C_B could be identified in analyzing the spectra. The sharper magnetic sextet A and the doublet C_A were assigned to Fe^{3+} ions at the tetrahedral A-sites and the broadened sextet B and the doublet C_B to Fe^{3+} and Fe^{2+} at the octahedral B-sites.

The infrared absorption spectra were recorded at room temperature using the solid potassium bromide method. The spectra were taken employing a Perkin-Elmer spectrometer in the range from 4000 to 200 cm^{-1}.

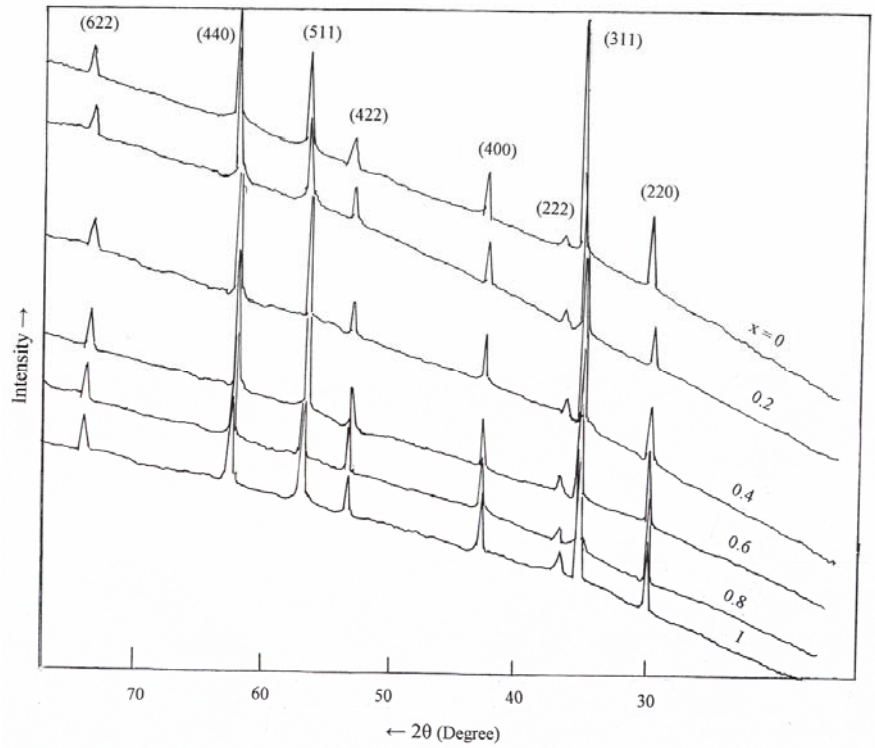

Fig. (1): The X-ray diffraction patterns of the $Ni_{0.5}\ Zn_{0.5}\ Cr_x\ Fe_{2-x}\ O_4$ ferrites.

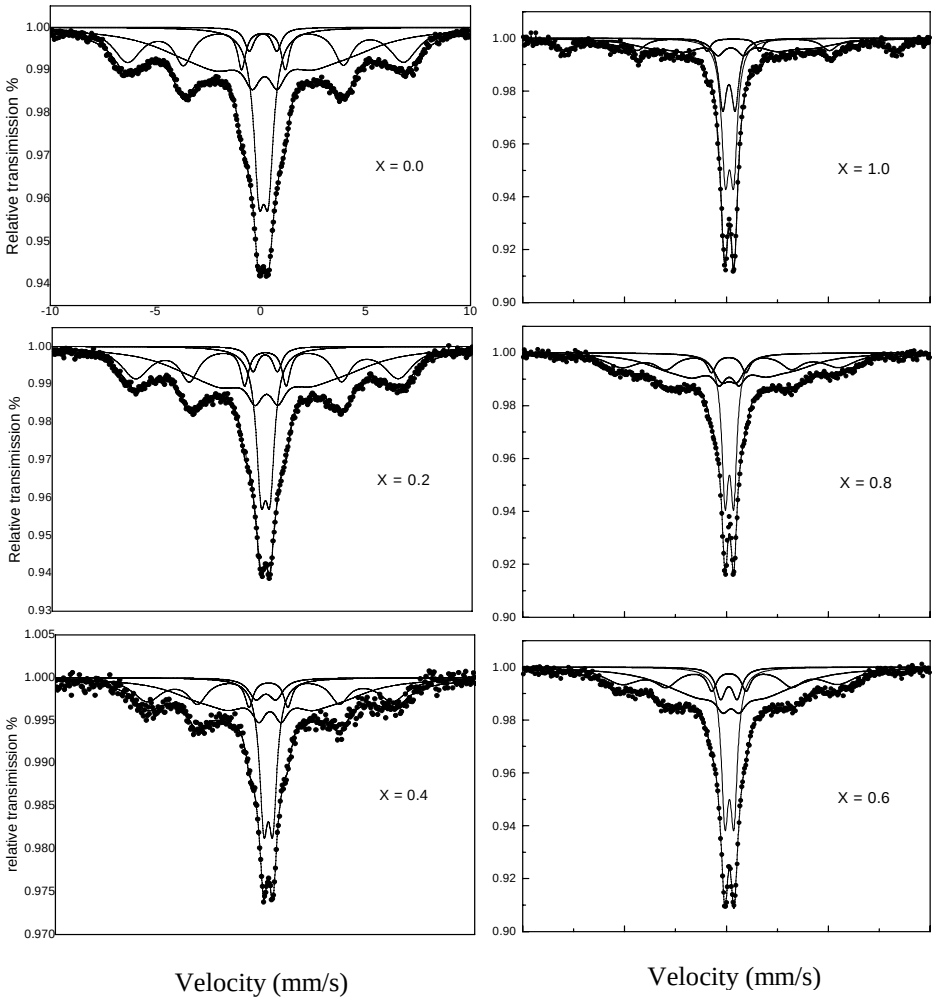

Fig. (2): The Mössbauer spectra of the system $Ni_{0.5}Zn_{0.5}Cr_xFe_{2-x}O_4$., obtained at room temperature for the indicated samples**.**

3. Results and Discussion:

3.1. Mössbauer spectra:

Figure (2) shows the room temperature Mössbauer spectra of the $Ni_{0.5}Zn_{0.5}Cr_xFe_{2-x}O_4$ ferrites. The spectra show a broadened sextet component and a central paramagnetic phase C for all samples. This behaviour is due to statistical fluctuations in the distribution of magnetic and nonmagnetic ions. The phase C arises from those Fe^{3+} ions, which are located within regions,

which are so small (particle size) that they behave superparamagnetically [10, 11]. The obtained results from the fits (as two sextets and two doublets) are given in Table (1). It is clear that the paramagnetic phases area of C_A and C_B increase with increasing the Cr^{3+} content x. This increase may be due to increasing the content of the diamagnetic ions; Ni^{3+} and Cr^{4+} in the samples by the fast hopping process; $Fe^{3+} + Ni^{2+} \leftrightarrow Fe^{2+} + Ni^{3+}$, $Fe^{3+} + Cr^{3} \leftrightarrow Fe^{2+} + Cr^{4+}$ and/or $Cr^{4+} + Ni^{2+} \leftrightarrow Cr^{3+} + Ni^{3+}$ [5], where Ni^{3+} migrates into the A-sites and Cr^{4+} remains in the B-sites.

Table (1): The Mössbauer parameters of the system $Ni_{0.5}Zn_{0.5}Cr_xFe_{2-x}O_4$, where ε_Q, δ, $\Gamma_{1,6}$ and A_0 are the quadrupole shift (or the quadrupole doublet splitting), isomer shift, outermost linewidth and fractional area of each (site) subspectrum, respectively.

X	Sites	ε_Q (mm/s)	δ (mm/s)	$\Gamma_{1,6}$(mm/s)	A_0
0	A	0.1	0.19	1.64	0.29
	B	0.11	0.26	4.67	0.49
	C_A	1.31	0.13	0.54	0.02
	C_B	0.46	0.15	1.11	0.2
0.2	A	0.07	0.19	1.66	0.28
	B	0.14	0.28	4.45	0.47
	C_A	1.16	0.14	0.54	0.04
	C_B	0.44	0.16	1.01	0.21
0.4	A	0.06	0.2	1.68	0.29
	B	-0.02	0.23	3.71	0.43
	C_A	0.96	0.14	0.83	0.05
	C_B	0.44	0.15	0.59	0.23
0.6	A	0.06	0.15	2.14	0.27
	B	-0.02	0.22	3.91	0.41
	C_A	0.81	0.12	0.57	0.08
	C_B	0.43	0.15	0.74	0.24
0.8	A	0.09	0.15	1.96	0.26
	B	0.1	0.18	3.17	0.34
	C_A	0.76	0.13	0.97	0.11
	C_B	0.41	0.15	0.4	0.29
1	A	-0.13	0.25	1.41	0.20
	B	0.1	0.29	2.93	0.29
	C_A	0.61	0.12	0.45	0.18
	C_B	0.40	0.15	0.97	0.33
Error		± 0.02	±0.02	±0.02	± 0.02

The isomer shift values δ for Fe ions at the A-sites δ_A and B-sites δ_B (Table 1), lie between 0.13 and 0.29 mm/s, which is consistent with Fe^{3+} ions in spinel ferrites [7, 8]. The absolute quadrupole shift values ε_Q of the magnetic sites A and B, ε_{QA} and ε_{QB}, lie between 0.02 and 0.14 mm/s (Table 1). The change of sign may originate from the angular factor [12]. Generally, the ε_{QA} arises from the asymmetrical charge distribution surrounding Fe^{3+} ion and the ε_{QB} has a trigonal point symmetry and exhibits an electric field gradient EFG along (111) direction. However, the relatively high values of ε_{QA} and ε_{QB} may be due to the chemical disorder of the samples, i. e. existing cations of different charges and radii in the sublattices. The relatively high values of δ_B and ε_{QB}, may be due to the mixed valency states between Fe^{2+} and Fe^{3+} ions.

The doublet structure is due to the quadrupole reaction of ^{57}Fe nuclei located on the A- and B-sites with EFG at these places. Thus the value of quadrupole doublet splitting ε_Q can provide information concerning the symmetry of the crystal lattice and its local distortions. The existence of two quadrupole doublets C_A and C_B, as shown in Fig. (2), was observed previously [13, 14]. This may arise from the random distribution of cations of different charges and radii on the A- and B-sites, which affects EFG. C_A and C_B may result as a consequence of the trigonal distortion of the B-site oxygen coordination i.e. the deformation of the $3d^5$ shells. This trigonal distortion is confirmed by the high values of the oxygen positional parameter *u* (sec 3.3). It is known that the standard value of *u* is 0.375 [15], whereas the obtained values are around 0.4. However, the quadrupole splitting values ε_Q of C_A and C_B decrease versus x (Table 1). This decrease may be due to decreasing the number of Fe^{3+}-O^{2-} bonds, in the sublattices by the substitution process. This may be explained by plotting the relation between both ε_{QA} and ε_{QB} and *u* as shown in Fig. (3a). This shows that both ε_{QA} and ε_{QB} decrease with increasing *u*. Hence, an important contribution to EFG arises from *d* electron covalence of the Fe^{3+}-O^{2-} bond. As illustrated by the supertransferred hyperfine field, the electrons transfer from the oxygen *p* orbitals into the Fe^{3+} *d* orbitals. This transfer causes a slight deformation of the spherical symmetry of the 3*d* electron charge density, resulting in a significance contribution of the EFG [16]. Consequently, decreasing the number of the Fe^{3+}-O^{2-} bonds decreases the values of ε_Q at the A- and B-sublattices.

The distribution of Fe^{3+} ions amongst the A- and B-sublattices can be understood from plotting the relation between the area ratio of B- to A-site subspectra and (molar ratio) x as illustrated in Fig. (3b). The decrease of this ratio against x clears that the substitution process often reduces the Fe^{3+} number in the lattice at the expense of the number of Fe^{3+} ions at the B-

sublattice. It is well known that the Zn^{2+} ions exclusively occupy the A-sites [1-6] and the Cr^{3+} ions the B-sites and the preferred site for the Ni^{2+} ions is the B-sites [6-8]. Consequently the cation distribution can be estimated, as given in Table (2), using the site preference of elements and the ratio of area under the well resolved subspectra belonging to the A and B sublattices. The outermost line width $\Gamma_{1,6}$ of the magnetic sites (component) B decreases with x, whereas that of the magnetic sites (component) A increases for $x \leq 0.6$ and decreases thereafter (table 1). This may be attributed to the change of the tetrahedral and octahedral environments of the Fe^{3+} ion at the A- and B-site, i. e. the cations distributions (Table 2).

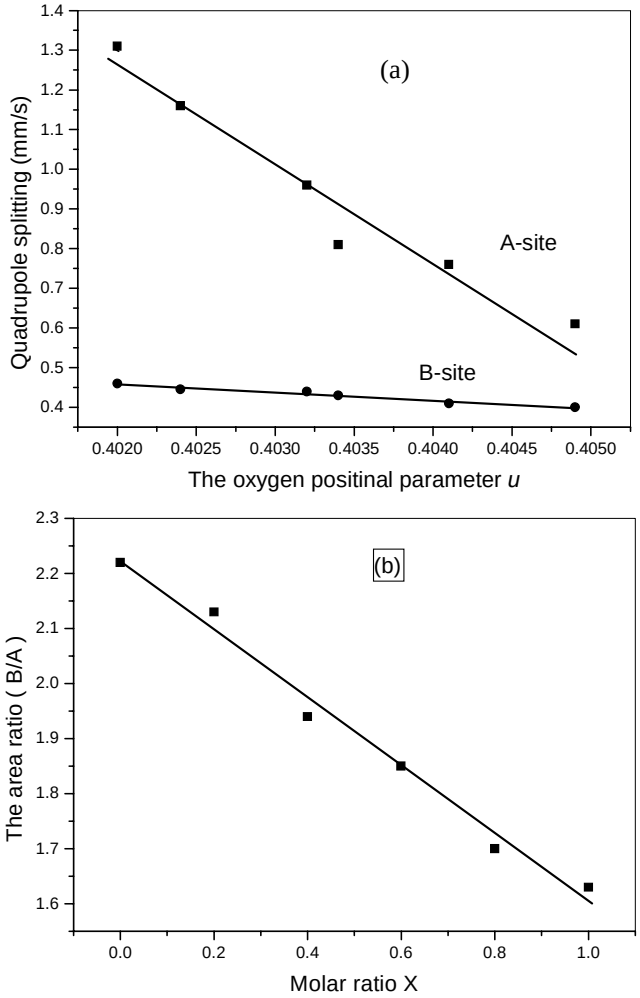

Fig.(3): The variation of (a) The quadrupole doublet splitting of the A-sites ε_{QA} and B-sites ε_{QB} against the oxygen positional parameter ***u***, and (b) the area ratio of the B- to the A-site against x.

The behavior of hyperfine magnetic field *H* at A- sites (H_A) and B-sites (H_B) as functions of Cr^{3+} content x is shown in Fig. (4a). H_A was found to be greater than H_B, where they decrease for $x \leq 0.6$ and increase thereafter. The decrease of H_A and H_B can be understood on the basis of decreasing the magnetic superexchange interaction between and within the sublattices due to the reduction of Fe^{3+} number. It is necessary to take not only the A-B superexchange but also the B-B supertransferred hyperfine interactions into account. In the cation distribution (Table 2), Zn^{2+} ions are non-magnetic and do not contribute to the nuclear magnetic field. Also, the Fe^{3+}-O^{2-}-Fe^{3+} superexchange interaction is higher than the Fe^{3+}-O^{2-}-Ni^{2+}, Ni^{2+}-O^{2-}-Fe^{3+}, and Fe^{3+}-O^{2-}-Cr^{3+} [15,17]. As a result, H_A and H_B decrease with increasing Cr^{3+} content instead of Fe^{3+} ions, i. e. decreasing the number of the magnetic bonds Fe^{3+}_A -O^{2-}-Fe^{3+}_B. Increasing H_A and H_B, for $x \geq 0.8$, may be attributed, in addition to the magnetic superexchange interactions within the sublattice, to the supertransferred A-A and B-B magnetic hyperfine interactions between the magnetic Fe^{3+}, Ni^{2+} and/or Cr^{3+} ions inter the A- and B-sublattices. It may arise from a ferromagnetic interaction between the magnetic ions within the sublattice. This increase agrees with that observed previously in Cu-Cr ferrite [6]. The spontaneous magnetization *Ms* of the bulk ferrimagnetic material was calculated as stated previously [18, 19]. The calculated negative *Ms* Values decrease against x, as shown in Fig. (4b), indicates that the direction of Ms is from A to B-sites. The behaviour of Ms Values against x is similar to that of Al-ferrites [20].

Table (2): Cation distribution in the ferrite system $Ni_{0.5}Zn_{0.5}Cr_xFe_{2-x}O_4$.

X	A-site	B-site
0	$Zn_{0.38}Fe_{0.62}$	$Zn_{0.12}Ni_{0.5}Fe_{1.38}$
0.2	$Zn_{0.41}Fe_{0.59}$	$Zn_{0.09}Ni_{0.5}Cr_{0.2}Fe_{1.21}$
0.4	$Zn_{0.46}Fe_{0.54}$	$Zn_{0.04}Ni_{0.5}Cr_{0.4}Fe_{1.06}$
0.6	$Zn_{0.5}Ni_{0.01}Fe_{0.49}$	$Ni_{0.49}Cr_{0.6}Fe_{.91}$
0.8	$Zn_{0.5}Ni_{0.06}Fe_{0.44}$	$Ni_{0.44}Cr_{0.8}Fe_{0.76}$
1	$Zn_{0.5}Ni_{0.12}Fe_{0.38}$	$Ni_{0.38}Cr_1Fe_{0.62}$

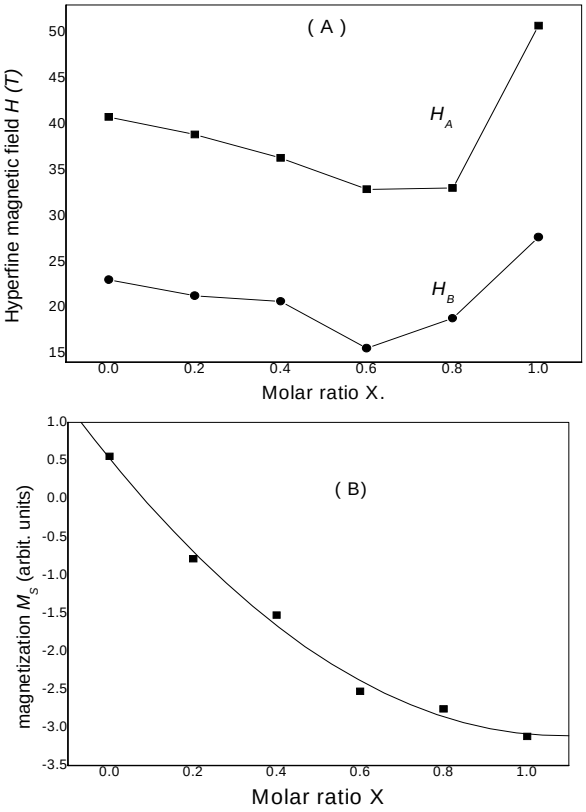

Fig.(4): The x dependence of (a) the hyperfine magnetic field of the A-site H_A and the B-site H_B and (b) the calculated spontaneous magnetization M_s.

3.2. Infrared spectra.

The most interesting feature of this study is the IR spectra as shown in Fig. (5). The results of IR studies are listed in Table (3). The two strong absorption bands, ν_1 and ν_2 are observed and assigned to the complexes of Fe^{3+}-O^{2-} at the A-site and of Fe^{3+}-O^{2-} and Cr^{3+}-O^{2-} at the B-site vibrational modes [17, 20-23]. The change in band positions is due to the change in the Fe^{3+}-O^{2-} internuclear distances for the A- and B-sites. Fig. (5) and Table (3) clear that the bands ν_1 and ν_2 shift towards the high energy with increasing Cr^{3+} substitution for Fe^{3+} ions. This may be explained on the basis of decreasing the concentration of Fe^{3+} ions amongst the A- and B-sites, which cause increasing the metal-oxygen stretching vibrational energies and cause decreasing the B-site ionic radius and reducing the size of the unit cell i.e. the lattice parameter *a* (sec. 3.3) [9]. The band ν_3 results from the splitting of the band ν_2 by the increasing presence of the Fe^{2+} ions at the B-site. Thus the band

ν_3 can be assigned originally to the Fe^{2+}-O^{2-} complexes and to the divalent metal ion-oxygen complexes in the B-sites [19-23]. The intensity of the band ν_3 increases with increasing Cr^{3+} concentration at B-sites due to the increasingly existence of Fe^{2+} resulting from the hopping process [5].

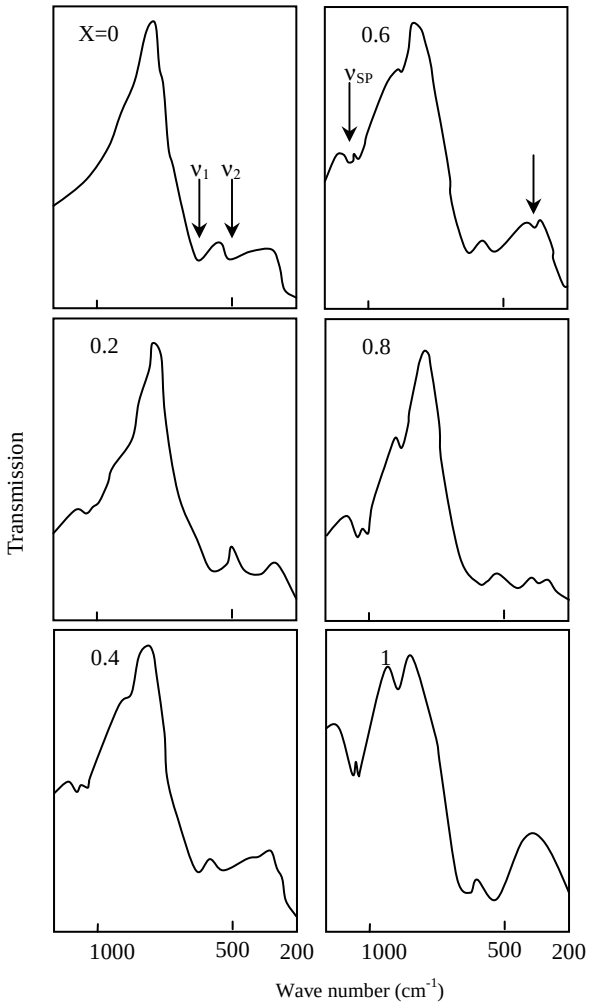

Fig. (5): The infrared transmittance spectra for the studied samples.

Table (3): The absorption band positions ν_n and their intensities I_n (n = 0, 1, 2, 3 and SP), SP denotes to splitting and Sh to Shoulder.

X	ν_{SP} (cm^{-1})	I_{SP}	ν_0 (cm^{-1})	I_0	ν_1 (cm^{-1})	I_1	ν_2 (cm^{-1})	I_2	ν_3 (cm^{-1})	I_3
0	-----	---	---	---	577	13	454	14	-----	---
0.2	1084-1043	26	Sh	---	548	13	395	17	-----	---
0.4	1082-1042	43	881	40	585	14	471	19	344	20
0.6	1082-1043	46	880	32	592	15	484	22	340	27
0.8	1082-1041	28	882	63	562	17	438	24	341	29
1	1082-1040	52	880	82	601	21	496	27	342	33
	±2	±2	±2	±2	±2	± 2	±2	± 2	±2	± 2

Two bands ν_0 and splitting band ν_{SP} appeared around ν_1 and become more pronounced with increasing Cr^{3+} ions content (Table 3). The band ν_0 was observed in the spectra of the Co-Ni ferrites and assigned to the intrinsic vibrations of the tetrahedral group [24, 25]. Some authors [21, 26], using IR and Raman spectra, reported that the peak ν_0 is generally found very intense in the oxide spinels (675 cm^{-1} in Fe_3O_4). They assigned it to the breathing mode of the tetrahedral A-sites or to a compound due to distribution of particle morphologies. Two side bands around ν_1 (600 cm^{-1}) were found in studying Ni-Zn ferrites [26], and assigned to the presence of Fe^{2+} ions in both A- and B-sites. In our case, the two bands ν_0 and ν_{SP} are clearly dependent on the statistical distribution of the cations amongst the A- and B-sites and on the Cr^{3+} ion concentration at B-site. The splitting band ν_{SP} appeared in studying Co-Zn ferrite [27], and was assigned to the greater concentration of Fe^{2+} ions and to the distortion of the spinel lattice. In our system, the band ν_{SP} can be assigned to the Cr^{4+}-O^{2-} complexes and to the local distortion of the cubic spinel lattice [26, 27]. Actually the bands ν_3 and ν_{SP} result from the splitting of the band ν_2 and are characteristic of the Jahn-Teller effect of the ions Fe^{2+}, Ni^{2+} and/or Cr^{4+} at the B-sites [24]. The intensity of the band ν_{SP} increases with increasing chromium addition. This reveals increasing the number of the Cr^{4+} ions at the B-sites by the hopping process. The bands ν_0 results from the splitting of the band ν_1 by the Jahn-Teller effect of the Fe^{2+}, Cr^{4+} and/or Ni^{2+} ions at A- -sites [24].

The refractive index *R* and the velocity *V* of the IR waves in the samples can be estimated from the relation [21, 28]:

$$\frac{E_t}{E_{ab}} = \frac{C}{V} = R$$

where E_t is the transmitted energy, E_{ab} the absorbed energy and C the velocity of light. The obtained values of R and V, as shown in Fig. (6a), indicate that the refractive index decreases, whereas the velocity of IR increases against x. The jump rate J of the lattice vacancies may be estimated from the relation [21, 28]: $J = \nu e^{E/kT}$, where ν is the frequency of the vibration, k the Boltzmann constant, $E = h\nu = V/\lambda$, h is the Planks constant and λ the IR wavelength. Fig. (6b) illustrates that the jump rate J of the lattice vacancies increase with increasing the Cr^{3+} content (x). The increase of the absorbed energy at ν_1 leads to decreasing the refractive index R with x. The substitution process x increases the Fe_A^{3+}- O^{2-} bond length d_{AL} (table 4) and weakens the B-B superexchange interactions which leads to vibrating the lattice at high frequency with the incident IR waves and to increasing the IR wave velocity V inside the samples. Increasing the jump rate J is attributed to increasing the cation vacancies by introducing the smaller Cr^{3+} ions into the B-sublattices. It may be attributed to the formation of the larger ions Fe^{2+} (0.76 Å) by the hopping process. The formation of larger ions increases the lattice vacancies and increases the jump rate [29].

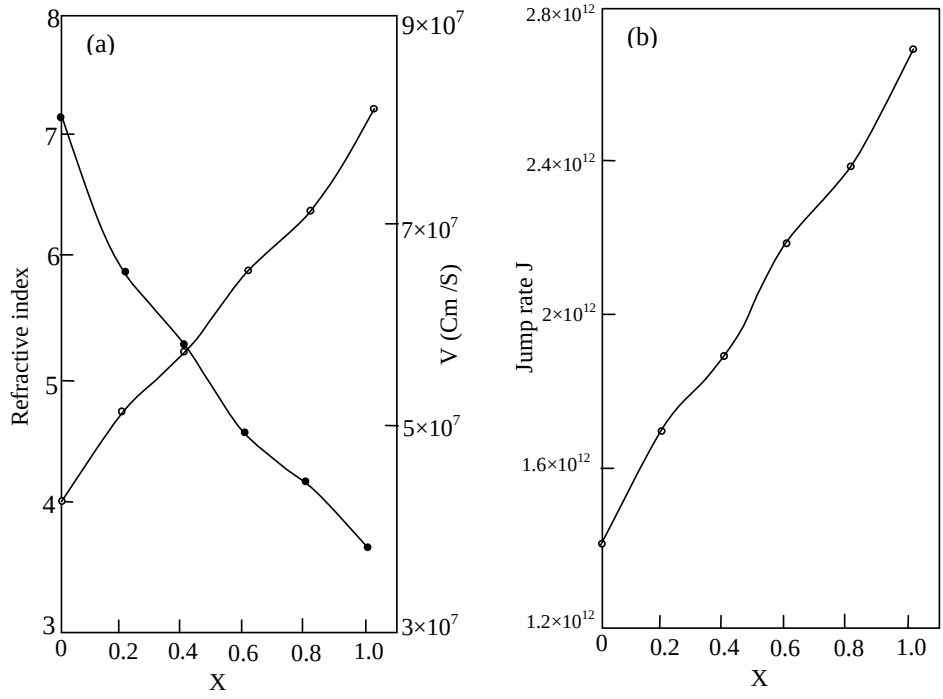

Fig.(6): The effect of the Cr3+ concentration x on (a) the IR refractive index R and velocity V, and (b) the jump rate of the cationic vacancies.

3.3. X-ray analysis

The chromium content x dependence of the theoretical density D_x is shown in Fig. (7a), and of the bulk density D and the porosity P in Fig. (7b). It is shown that D_X and P decrease, whereas D increases with x. These variations of P and D with x may be attributed to the decrease of the oxygen vacancies, which play a predominant role in accelerating densification [30]. The decrease of D_X may be assigned to the substitution of the lighter ions Cr^{3+} (51.996) instead of Fe^{3+} (55.847). For obtaining the true lattice parameter a_0, the measured lattice parameter a was plotted versus the Nelson-Riley function [30-32];

$$F(\theta)=\frac{1}{2}\left(\frac{\cos^2\theta}{\sin\theta}+\frac{\cos^2\theta}{\theta}\right)$$

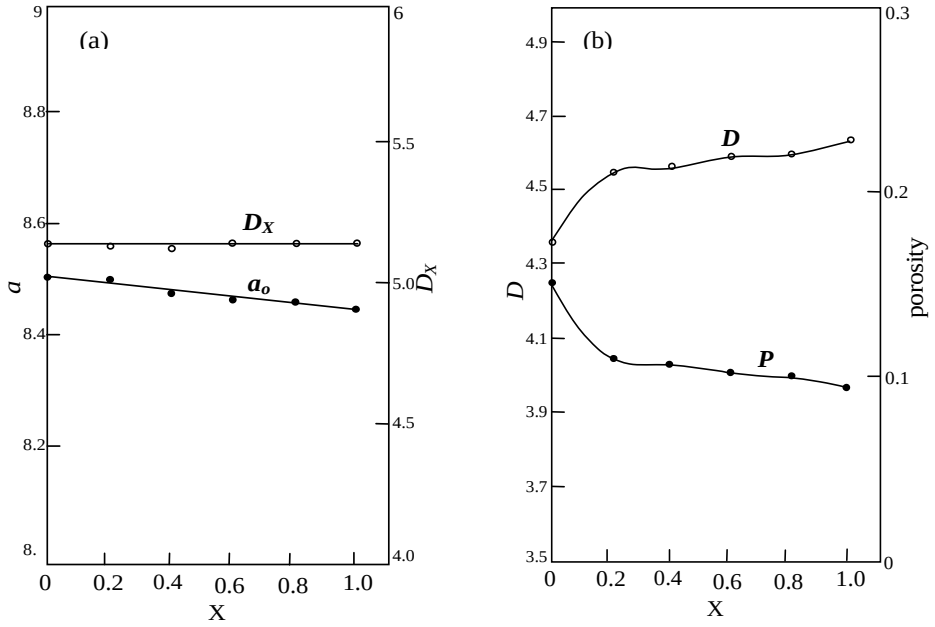

Fig.(7): The variation of (a) the average lattice parameter a_o and the theoretical density D_x , and (b) the bulk density D and the porosity P, against x.

The plots are straight lines with increasing trend, as shown in Fig. (8). The true lattice parameter a_0 can be obtained by extrapolating the lines to F (θ)= 0 at θ =90°. The obtained values of a_0 are listed in Table (4). The variation of a_0 against x is shown in Fig (7). a. It is clear that a_0 decreases with increasing the Cr^{3+} content in the samples. This decrease is assigned to the

substitution of the smaller radius Cr^{3+} ion (0.64 Å) for Fe^{3+} ion (0.67 Å). The deduced cation distribution (Table 2) may be confirmed by using it for calculating the theoretical lattice parameter a_{th} as indicated previously [33].

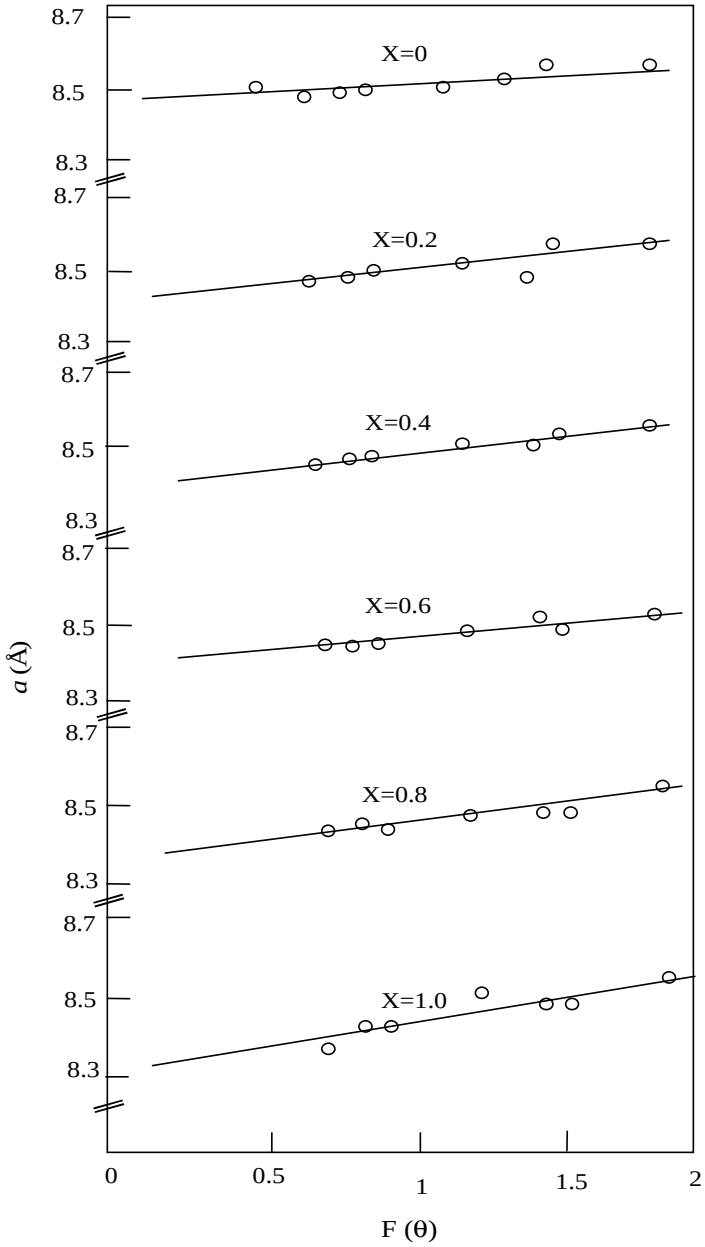

Fig. (8): The relation between Nelson-Riley F (θ) and the lattice parameters *a*.

The calculated values of a_{th} are given in table 4. The comparison between the obtained values for both a_0 and a_{th} (Table 4) illustrate that their values are approximately equal, which confirm the estimated cation distribution (Table 2). The oxygen parameter *u* can be obtained as indicated previously [33-37]. The mean ionic radius of the A-site r_A and of the B-site r_B may be calculated as indicated previously [27, 33-37].

Table (4): The calculated X-ray parameters; the tetrahedral and octahedral bond length, d_{AL} and d_{BL}, the tetrahedral edge d_{AE}, the shared and unshared octahedral edge d_{BE} and d_{BEU} and the true and theoretical lattice parameters a_0 and a_{th}.

x	d_{AL} (Å)	d_{BL} (Å)	d_{AE} (Å)	d_{BE} (Å)	d_{BEU} (Å)	a_0 (Å)	a_{th} (Å)	L_A (Å)	L_B (Å)
0	2.095	1.952	3.421	2.518	2.986	8.4	8.4	3.667	3.006
0.2	2.118	1.939	3.458	2.476	2.987	8.394	8.389	3.642	2.974
0.4	2.147	1.925	3.505	2.428	2.991	8.382	8.378	3.634	2.968
0.6	2.15	1.922	3.51	2.42	2.990	8.384	8.379	3.631	2.965
0.8	2.154	1.92	3.517	2.418	2.991	8.368	8.366	3.623	2.958
1	2.144	1.9	3.492	2.379	2.992	8.334	8.35	3.596	2.936

The calculated values of *u*, r_A and r_B are drawn against (molar ratio) x as shown in Fig. (9a). It is shown that r_B decreases noticeably as function of x, whereas *u* and r_A increase slowly. This observation may be due to the correlation between the ionic radius and the lattice parameters [26, 36]. The decrease of r_B is due to the replacement of the Fe^{3+} ions at the octahedral B-sites by the smaller radius Cr^{3+} ions. The increase of r_A may be due to the increasingly migration of the larger Zn^{2+} (0.82 Å) and Ni^{2+} ions (0.72 Å) to the A-sites (Table 2). The little increase of *u* is a direct consequence of increasing the trigonal distortion of the B-site oxygen coordination. Introducing the larger volume Zn^{2+} and Ni^{2+} ions into the A-sites increases the trigonal distortion of the B-site oxygen coordination during accommodation these ions.

Using the values of a_0 and *u* the tetrahedral and octahedral bond length (d_{AL} and d_{BL}), the tetrahedral edge d_{AE} and the shared and unshared octahedral edge (d_{BE} and d_{BEU}) may be calculated as indicated previously [33-36]. The calculated values are given in Table 4. It is clear that d_{AL}, d_{AE} and d_{BEU} increase with x, which is ascribed to the increasing migration of the larger ions Zn^{2+} and Ni^{2+} into the A-sublattices with *x* (Table 2). However, the decrease of d_{BL} and d_{BE} is attributed to the introducing the smaller radius of the added Cr^{3+} ions into the B-sites as compared with the substituted Fe^{3+} ions.

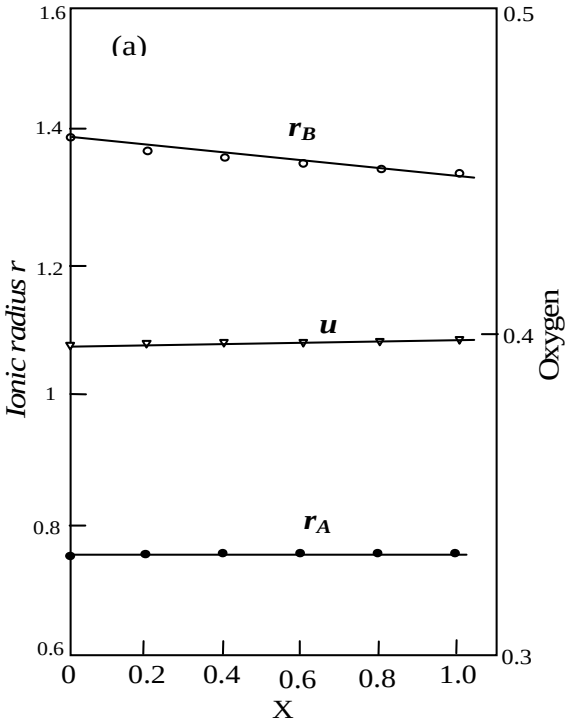

Fig.(9): The behaviour of the ionic radius of the A-site r_A and of the B-site r_B and the oxygen positional parameter u as functions of x.

The distance between the magnetic ions L (the hopping length) of the A-sites can be obtained by $L_A = a_0\sqrt{3}/4$ and of the B-sites by $L_B = a_0\sqrt{2}/4$ as given in table 4 [36, 38]. Decreasing L_A and L_B with x, as given in Table 4, may be due to reducing the unit cell size (a_t). This may be attributed to the introducing of the smaller size magnetic Cr^{3+} ions into the B-sublattice and migration the magnetic Ni^{2+} ions into the A-sublattices, which make the magnetic ions approach to each other and decrease the hopping length between them. The dependence of the magnetic fields H_A and H_B on the hopping lengths L_A and L_B, respectively, is shown in Fig (10). H_A and H_B reflect the same behavior with L. Their highest values are at the least distance between the ions, where they decrease sharply to a minimum value for each. This minimum value depends on the distance L at the corresponding site. However, increasing the distance L between the site-ions increases the hyperfine field at this site with a slow increasing rate. This may be explained as follows; (1) it is known that the ions Ni^{3+} and Cr^{4+} are nonmagnetic, the magnetic moment of Fe^{2+} ion is less than that of Fe^{3+} ion and the hopping

process between the magnetic cations produces Ni^{3+}, Cr^{4+} and Fe^{2+} ions. (2) Introducing the highest concentration of the smaller Cr^{3+} ions (the least L) into the B-sublattices creates a cation vacancies, which can block the hopping process between Fe^{3+} and Ni^{2+}, (3) The high content of Cr^{3+} can activate the hopping process between Cr^{3+} and both Ni^{3+} and Fe^{2+} transforming them to Ni^{2+} and Fe^{3+} ions and giving rise the highest magnetic fields of the sublattices, (4) Hence, decreasing the Cr^{3+} concentrations (increasing L) increases the hopping process between Fe^{3+} and Ni^{2+}, therefore H_A and H_B decrease to a critical value, (5) above this value the concentration of Fe^{3+} ions increase instead of Cr^{3+} ions i. e. the number of the magnetic bonds Fe^{3+}- O^{2-} - Fe^{3+} increase and then H_A and H_B increase.

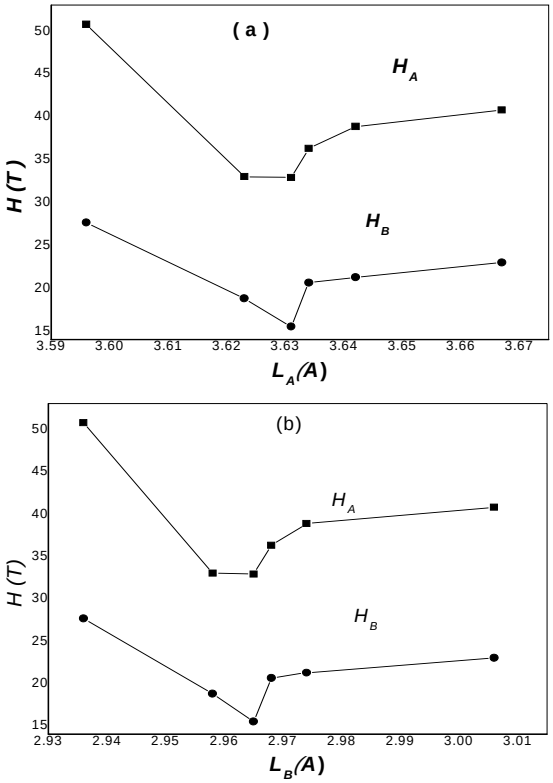

Fig. (10): The dependence of the hyperfine fields H_A and H_B on the distance between the magnetic ions at the A-sites L_A and B-sites L_B, respectively.

4. Conclusion:

X-ray and IR studies proved the spinel structure of the studied system. The Mössbauer spectra have been fitted to two magnetic sextet A and B and two quadrupole doublets C_A and C_B. The line widths and the quadrupole doublet splitting of C_A and C_B showed a dependency of the cr^{3+} ion content.

Also the Cr^{3+} ion contents were found to affect on the area ratio of the B- to A-sites, the hyperfine magnetic field at A- and B-sites, H_A and H_B, and the magnetization. The cation distribution has been estimated by X-ray study. The Mössbauer and IR studies reveal the existing of Fe^{2+} ions in the sublattices by the hopping process. Five IR absorption bands are reported in the range from 1100 to 200 cm^{-1}. The additions of Cr^{3+} ions change the band positions and shift the bands ν_1 and ν_2 towards the high-energy side. The velocity of the IR waves and the jump rate of the lattice vacancies were found to increase, whereas the IR refractive index decreases against (molar ratio) x. From X-ray studies, the A-site ionic radius, bond length and edge, the B-site unshared edge and the oxygen positional parameter were increasing with increasing x, whereas the B-site radius, the bond length and shared edge, the hopping lengths, and the true lattice parameter were decreasing. The magnetic fields H_A and H_B revealed a dependency on the x as well as hopping lengths L_A and L_B at the A- and B-sites, respectively.

Note:

This article is reinterpretation of the article published in Turkish Journal of Physics,[39].

References:

1. N. Rezlescu, E. Rezlescu, C. Pasnicu and M. L. Craus, *J. Phys. Condens. Matter*. **6**, 5707 (1994).

2. C. Sung, W. C. Ki, S. Y. An and S. Lee, *J. Magn. Magn. Mater*. **215**-216, 213 (2000).

3. Yu G. Chukalkin and V. R. Shtirts, *Phys. Stat. Sol*. (a) **160**, 185 (1997).

4. J. C. Waerenborgh, M. O. Figuered, J. M. P. Cabrol and L. C. J. Pereiro, *J. Solid State Chem*. **111**, 300 (1994).

5. A. K. Singh, T. C. Goel and R. G. Mendiratta, *J. Magn. Magn. Mater*. **125/2**, 121 (2003).

6. M. A. Amer, M. A. Ahmed, M. K. El-Nimr and M. K. Mustafa, *Hyperfine Interactions* **96**, 91-98 (1995).

7. A. M. Sankpal, S. S. Suryavanshi, S. V. Kakatkar, G. G. Tengshe, R. S. Patil, N. D. Chaudhari and S. R. Sawant, *J. Mag. Mag. Mater*. **186/3**, 349 (1998).

8. H. N. Ok, K. S. Baek and E. J. Chsi, *Phys. Rev*. B **40**, 84 (1989).

9. M. A. Amer, *Phys. Stat. Sol*. (a) **151**, 205 (1995).

10. E. De Grave, R. Van Leerberghe, C. Dauwe, A. Covaert and J. De Sitter, *J. Phys. Collog*. **37**, c6-97 (1976).

11. E. De Grave, A. Covaert, D. Chambaere and C. Robbrecht, *J. Phys. Collog*. **40**, C2-669 (1979).

12. H. N. Ok and B. J. Evans, *Phys. Rev*. **B 14**, 2956 (1976).
13. R. Van Leerberghe and R. E. Vandenberghe, *Hyperfine Interactions* **23**, 75 (1985).
14. R. Gerardin, A. Randani, C. Gleitzer, B. Gillot and B. Durand, *J. Solid State Chem.* **57**, 215 (1985).
15. L. K. Leung, B. J. Evans and R. Renaudin, *Phys. Rev*. **B, 29** (1973).
16. M. K. Fayk. F. M. Sayed Ahmed, S. S. Ata-Allah, M. K. El-Nimr and M. F. Mostafa, *J. Mater. Sci*. **27**, 4813 (1992).
17. J. S. Baijal, D. Kothari, S. Phanjoubam and C. Prakash, *Solid state commun*. **69**, 277 (1989).
18. M. A. Amer, *Phys. Stat. Sol*. **(a) 145**, 157 (1994).
19. M. I. Baraton, V. Lorenzelli, G. Busca and R.Jj. Willy, *J. Mater. Sci. Letters* **13**, 275 (1994).
20. M. A. Amer, *Hyperfine interactions* **131**, 29 (2000).
21. O. M. Hemeda, *J. Mag. and Mag. Mater*. **281**, 36 (2004).
22. D. Ravinder and V. Kumar, *Bull. Mater. Sci*. **24**, 505 (2001).
23. O. M. Hemeda and M. I. Abd EL-Ati, *J. Mag. Mag. Mater*. **51**, 42 (2001).
24. S. A. Patil, S. M. Otari, V. C. Mahajan, M. G. Patil, A. B. Patil, M. K. Soudajar, B. L. Patil and S. R. Sawant, *Solid State Comm*. *78/1*, 39 (1991).
25. M. K. El-Nimr, M. A. Ahmed and M. A. El hiti, *J. Mater. Sci. Letters* **13**, 1500 (1994).
26. V. A. Potokova, N. D. Zverv and V. P. Romanov, *Phys Stat. Sol*. **(a)12**, 623 (1972).
27. N. Z. Darwish, *Appl. Phys. Commun*. **13**, 243 (1994).
28. J. Neumann, M. O. Rowe, H. Veenhuis, R. Pankrath and E. Kratzig, *Phys. Stat. Sol*. **(b) 215**, R9 (1999).
29. O. M. Hemeda and M. M. Barakat, *J. Mag. Mag. Mater*. **323**, 127 (2001).
30. J. K. Srivastava, K. Muraleeharan and R. Vijayaraghavan, *J. Phys. Chem. Solids* **48**, n12, 1251 (1987).
31. J. B. Nelson and D. P. Riley, *Proc. Phys. Soc., London* **57**, 160 (1945).
32. O. M. Hemeda, M. A. Amer, S. Aboul-Enein and M. A. Ahmed, *Phys. Stat. Sol*. **(a) 156**, 29 (1996).
33. A. A. Yousif, M. E. Elzain, S. A. mazen, H. H. Sutherland, M. h. Abdallah and S. F. Mansour, *J. Phys. Condens. Matter* **6**, 5717 (1994).
34. O. Ravinder, *J. Appl. Phys*. **75**, 6121 (1994).
35. C. Arean, J. Blanco, J. Gonzales and M. Fernandez, *J. Matter. Sci. Lett*. **9**, 229 (1990).
36. P. V. Reddy and T. Seshegirirao, *J. Less-Common Metals* **75**, 255 (1980).
37. M. Abo El Ata, S. M. Attia and T. M. Meaz, *Solid State Sci*. **6**, 61-69(2004)
38. H. Pascard, A. Globus and V. Cabon, *J. Physique 38*, C1, 163 (1977).
39. M. Amer, S. Ata-Allah, T. M. Meaz, S. Aboul-Enein and M. Abd-Elhamid, *Turk. J. Physi. 29,163-177 (2005)*